Gondwana Research 106 (2022) 237–246

Contents lists available at ScienceDirect

Gondwana Research

journal homepage: www.elsevier.com/locate/gr

Preservation of the Iberian Tethys paleomargin beneath the eastern Betic mountain range

José Morales [a,b,*], Antonio Molina-Aguilera [a,b], Flor de Lis Mancilla [a,b], Daniel Stich [a,b], José Miguel Azañón [a,c], Teresa Teixidó [a], José Angel López-Comino [a,b], Benjamín Heit [d], Xiaohui Yuan [d], Antonio Miguel Posadas [a,e]

[a] Instituto Andaluz de Geofísica, Universidad de Granada, Campus de Cartuja, c/Prof. Clavera n° 12, 18071 Granada, Spain
[b] Departamento de Física Teórica y del Cosmos, Facultad de Ciencias, Universidad de Granada, Campus de Fuente Nueva, 18071 Granada, Spain
[c] Departamento de Geodinámica, Facultad de Ciencias, Universidad de Granada, Campus de Fuentenueva, 18071, Spain
[d] Deutsches GeoForschungsZentrum, GFZ, Telegrafenberg, 14473 Potsdam, Germany
[e] Departamento de Química y Física, Universidad de Almería, 04120 Almería, Spain

ARTICLE INFO

Article history:
Received 14 May 2021
Revised 17 November 2021
Accepted 10 January 2022
Available online 5 February 2022
Handling Editor: N. Rawlinson

Keywords:
Tethys paleomargin
South Iberian peninsula
Eastern Betic Cordillera
Crustal structure
P-wave Receiver Functions

ABSTRACT

We obtain P-wave receiver functions from teleseismic earthquake recordings at a dense seismic broadband transect, deployed along 170 km across the Betic mountain range in southeastern Spain. Migrated images show the crustal structure of the orogen in detail. In particular, they reveal the situation of the subducted Iberian paleomargin, with full preservation of the proximal domain and the ~50 km wide necking domain. Crustal thinning across the necking domain affects mainly the lower continental crust. The Variscan crust of the Tethys margin is bending downward beneath the Betics, reaching ~45 km depth, and terminates abruptly at a major slab tear. The distal domain of the paleomargin cannot be reconstructed, but the migrated section suggests that material has been exhumed through the subduction channel and integrated into the Betic orogen. This supports an origin of the HP-LT Nevado-Filabride units from subducted, hyperextended Variscan crust. According to our profile, the present-day eastern Betics appear to have a much more significant contribution from metamorphic Iberian crust than previously thought.

1. Introduction

Seafloor spreading around Iberia started in the mid Jurassic almost simultaneously in the Alpine Tethys and central Atlantic, and propagated also into the northern Atlantic in the Early Cretaceous (Stampfli et al., 2002, Schettino and Turco, 2010, Frizon de Lamotte et al., 2011). The Atlantic passive margin of Iberia has been extensively studied, often in comparison with the conjugate margin of Newfoundland, and found to show a magma-poor rifted architecture, characterized by a wide ocean-continent transition, the presence of hyperextended Variscan crust and the exhumation of serpentinized mantle (e.g. Peron-Pinvidic et al., 2013, Sutra et al., 2013). In turn, we know little about the Tethys continental margin of Iberia, which became involved in rollback of the Western Mediterranean subduction system (Lonergan and White, 1997, Faccenna et al., 2004), overthrust by the westward motion of the Alboran domain, and eventually integrated into the Betic mountain range or removed by slab tearing in the late stage of subduction (Mancilla et al., 2015b, 2018). Slab rollback and tearing in the Betics is apparently related to the intrusion of Si-K rich and Si-poor volcanics between 9-1 Ma, (Duggen et al., 2005; 2008), the development of ductile-brittle extensional detachments and exhumation of HP metamorphic rocks (Alpujarride and Nevado-Filabride complex) during middle Miocene to Quaternary (e.g. Martínez-Martínez et al., 2002; Booth-Rea et al., 2007; 2012), and the important crustal and lithospheric thinning and large epeirogenic uplift of the Betics and Rif since 8–6 Ma (Braga et al., 2003; Duggen et al., 2003; García-Castellanos and Villasenor, 2011).

The Betic range is traditionally divided into the Flysch units, the External Zones and the Internal Zones (Fig. 1, Balanyá and García-Dueñas, 1987). While the Internal Zones are composed mainly of metamorphic, Paleozoic and Mesozoic meta-sedimentary rocks, the External Zones preserve deformed Mesozoic to Miocene sedimentary rocks (Prebetic and Subbetic units), originally deposited onto the passive paleomargin (Fig. 1, García-Hernández et al., 1980). The collisional features in the Betics, result of ~200 km of roughly N-S convergence between mid-Oligocene and Late

* Corresponding author.
E-mail address: jmorales@ugr.es (J. Morales).

https://doi.org/10.1016/j.gr.2022.01.015

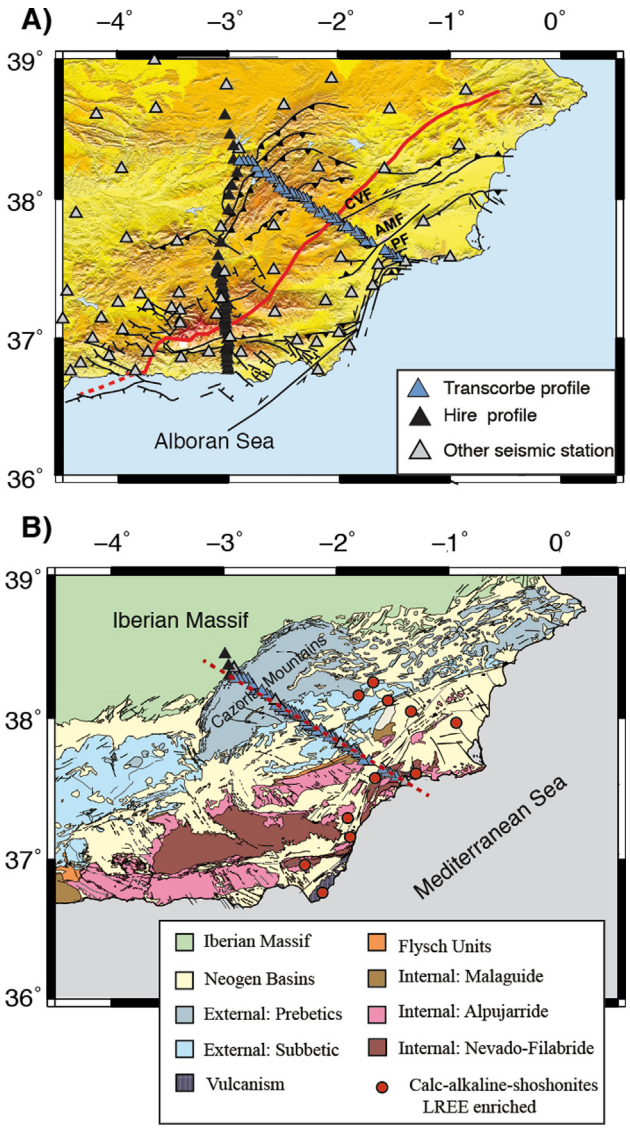

Fig. 1. A: Topography with the locations of the TransCorBe seismic profile (blue triangle) and a previous seismic profile HiRe (black triangles) together with other permanents and temporary stations deployed in the study area (grey triangles). We include the main faults and the probable location of tearing at the edge of the Alboran slab inferred by Mancilla et al. 2015a (red line and dashed red line); B: Geologic map with the main terranes and volcanism. Abbreviations: CVF: Crevillente Fault; AMF: Alhama de Murcia Fault; PF: Palomares Fault. (For interpretation of the references to colour in this figure legend, the reader is referred to the web version of this article.)

Miocene time and ~50 km of WNW-directed oblique convergence since the Late-Miocene, coexist with very significant extensional structures inducing a broad crustal stretching on the Internal Zones. Compared to other *peri*-Mediterranean orogens, the Betic Cordillera experiments a contractive reorganization since the late Miocene, causing folding, tectonic inversions and strike-slip faulting in the whole region. This event could be associated to the behaviour of the slab at depth (Faccenna et al., 2001a; Faccenna et al., 2001b; Vignaroli et al., 2008; Spakman et al., 2018).

So far, conjectures about the nature and deep architecture of the Tethys margin have to be developed from indirect observations. Some clues come from ultramafic and mafic rocks in the Nevado-Filabride complex of the internal zone of the Betics, that may be associated to serpentinized subcontinental mantle (Booth-Rea et al., 2005; Gómez-Pugnaire et al., 2012; Jabaloy et al., 2015) or Mesozoic oceanic lithosphere (Puga et al., 2017). Nevado-Filabride rocks (metapelites and metabasites) of continental origin experimented high-pressure, low-temperature (HP-LT) metamorphism (1.6 GPa to 2.2 GPa), suggesting a burial depth of 50–70 km (Augier et al., 2005; López-Sánchez-Vizcaíno et al., 2001; Behr and Platt, 2012; Dilissen et al., 2018; Santamaría-López et al., 2019). Such depths may indicate the involvement of Nevado-Filabride rocks in subduction, and hence their provenance from the extended continental margin. Conodont fossils provide further support for an assignment of the Nevado-Filabride unit to the Iberian margin (Rodríguez-Cañero et al., 2018). Such recent work is questioning the classic association of the Nevado-Filabride complex with the allochthonous Alboran domain, and instead suggests that the internal zone of the Betic range may have had a more complicated evolution, blending allochthonous elements with material from the Variscan margin (Booth-Rea et al., 2005; Gómez-Pugnaire et al., 2012; Jabaloy-Sánchez et al., 2018).

To obtain information on the internal structure of the Betic mountain range, we deployed a 170 km long, dense transect of three-component seismic broadband stations across the entire width of the orogeny (blue triangles, Fig. 1). The profile samples the different tectonic domains of the range, the internal and external zones, as well as the transition to the autochthonous Variscan foreland. The NW-SE trend of the profile is chosen perpendicular to the local trend of the orogen, but is actually also parallel to the Tethys spreading direction (Stampfli et al., 2002). In this study, we retrieve and migrate receiver functions for teleseismic P-waves, to image the position of principal discontinuities in the lithosphere. We expect that the length and direction of the profile are suitable for understanding the role and fate of the Iberia Tethys margin and the deep architecture of the Betics across the full width of the orogen.

2. Data and method

We analyse data from a 170 km long passive seismic transect which we named the TransCorBe profile (Trans Cordillera Bética; blue triangles in Fig. 1). 37 temporary seismic broadband stations from the Geophysical Instrument Pool at GFZ Potsdam form the backbone of the field experiment (blue triangles in Fig. 1, Morales et al. 2015). We complement the transect with three permanent 120 s-broadband stations (SESP, VALD, and MAZA stations, grey triangles, Fig. 1B) from the Instituto Andaluz de Geofísica (IAG, http://iagpds.ugr.es) and three temporary broadband stations from the Hire experiment (black triangles, Fig. 1, Mancilla et al. 2018). The TransCorBe profile operated from July 2013 to June 2015 and was deployed in NNW-SSE direction across the full width of the eastern Betic Cordillera, from the village of Mazarrón at the Mediterranean coast to the Iberian Massif in the interior of Spain. The typical distances between stations along the profile are ~3.5 km, which provides a sufficiently dense underground coverage for building images of the crustal seismic interfaces through P-wave receiver function analysis (i.e. Mancilla et al. 2018).

P-wave receiver functions (RFs) are time series that contain P-to-S-converted and multiply reverberated phases generated at seismic discontinuities underneath the recording stations (Vinnik, 1977; Langston, 1979). The RFs are obtained from three-component seismograms by deconvolving the vertical component from the horizontal components in the time window corresponding to the first P arrival and its coda. Ideally, deconvolution removes completely the effects of the source, teleseismic wave propagation, and the instrument response from the waveforms, and in the RFs there only remains the information related with the local earth structure beneath the station. In this study, we employ an iterative time domain deconvolution method (Ligorria

and Ammon, 1999) to extract RFs. We choose a Gaussian filter width factor of 2.5, which translates into receiver function pulses of around 1 s width. Prior to deconvolution, we rotate the horizontal and vertical components into the ray coordinate system, using the theoretical backazimuth and incident angles. In this way, we obtain the L (longitudinal), Q and T-components of the wavefield, to achieve the separation of P-waves (L) from vertically polarized (Q) and horizontally polarized (T) S-waves (see Mancilla et al. 2015a for processing details).

We calculate P-wave RFs for all stations of the TransCorBe profile from available recordings of teleseismic earthquakes with magnitude Mw > 5.5 located in the epicentral distance range between 30° and 90° (inset map in Fig. 2). The number of used RFs, with appropriate signal-to-noise ratio, for the temporary stations ranges from 68 to 5. The difference in the number of the receiver functions between stations is mainly due to technical problems at a few stations. In the case of permanent stations, we use four to six years of data (i.e. 159 RFs for SESP and 129 for VALD). The distribution of the earthquakes and azimuthal coverage for the temporary experiment can be observed in the inset panel of Fig. 2. The permanent stations used show similar azimuthal coverage, following the distribution of global seismicity. For some of the stations, the transverse RF-components (T) contain significant energy and we observe features that can be explained by dipping layers or anisotropy. In this study we will focus on the Q-components to obtain images of underground structure, however we additionally show T-components to corroborate heterogeneity of subsurface structures in several sections of the profile.

RFs along the TransCorBe profile show typically complex waveforms with several converted phases and some of them show signatures of dipping converters, suggesting complexity of the crustal architecture. We get a robust initial overview of the principal discontinuities from a representation of summation traces of the Q-components at each station along the profile (Fig. 2). To show in detail the quality of the data and to support this first approximation, we display Q and T-components of the RFs from some representative stations along the profile (Fig. 3a and b). RFs show great variability between stations along the profile in terms of complexity of the signals. For stations located directly on the Iberian Massif, or in the area of thin Prebetic units (approximately from stations TR30 to TR48), the Q-components of the RF's denote a relative simple structure, well defined by a constant and clear Pms phase (P-to-S conversion at the Moho) plus an evident intracrust discontinuity (green line, Fig. 2). No significant energy can be detected in the transverse components of the RFs for this sector (e.g. TR41 station, Fig. 3b).

The complexity of the RFs increases on both Q and T-components as we approach the central section of the profile, characterized by the transition between the external zones (Subbetic units) and the Alborán domain (Fig. 3b). A remarkable point is the presence of the Crevillente Fault (fault trace near station TR19). The mentioned complexity in this sector is evident for example in the Pms arrival time of the stacked RFs (Fig. 2) and in the Q and T-components (Fig. 3b) with a prominent step in the Pms delay time from 6 s (TR19) to 4.5 s (TR17) or 4 s (TR15). Significant energy is also detected in the transverse components in the RFs of this sector (Fig. 3b), whose characteristics may be explained by the presence of steeply dipping layers and/or anisotropy, which provides further evidences the complexity of this sector that is key to understand the crustal structure. In the Alboran's domain, the RFs are simpler with shallower Pms (less than 4 s of delay time), although some energy in the T-component indicates that the Moho is dipping towards the NW in this sector (Fig. 3c).

The dense spacing of seismic stations contributed to multifold underground coverage along the profile and allows building migration images and increasing the detail of subsurface positions of the crustal discontinuities with high spatial resolution using the common conversion point (CCP) stacking technique (Yuan, 2000). For this purpose, the RFs are migrated, i.e. back-projected along the incident ray paths, and then stacked into bins taking into account the increase of the Fresnel zone with depth (Yuan, 2000), as well as taking into account the coherence with the application of a phase-weighting factor (Schimmel & Paulssen 1997, Frassetto et al. 2010). We stack in the cross-section all the RFs amplitudes with piercing points inside a band with halfwidth of 20 km at both sides of the profile (Fig. 4a). The size of bins is 1 km along the strike of the profile and 2 km in depth. We afterwards apply spatial smoothing to the figure, using a Gaussian filter of 3 km. With this migration, we can delineate the variation of the Moho discontinuity and other intracrustal structures defined by strong seismic waves conversions. A modification of the IASP91 reference velocity model using crustal information from previous refraction profiles was used to

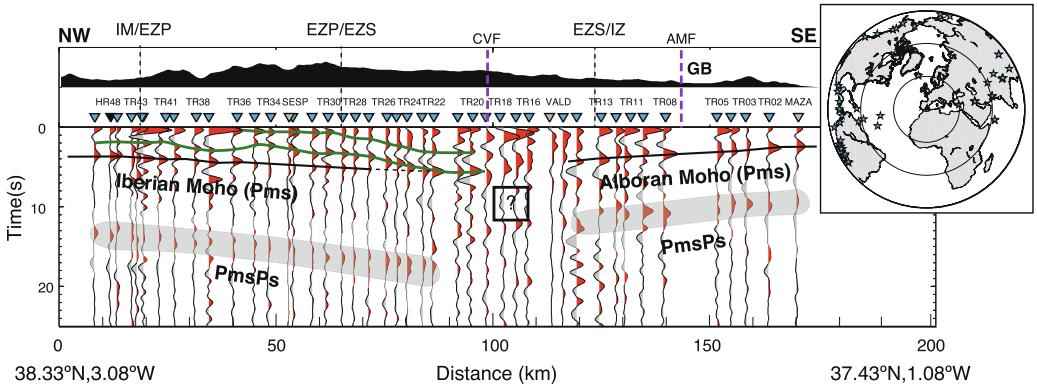

Fig. 2. Summation traces of the Q-components of RFs along the TransCorBe profile (red dashed line in Fig. 1). Blue triangles shows the position of the TransCorBe seismic stations used in the analysis with their name codes (TR); Grey triangle represent the location of permanent seismic stations used and black triangle represent seismic station belonging to another passive experiment "HiRe" (Fig. 1; Mancilla et al., 2018). All traces have been corrected for Ps-moveout prior to stacking. On top, the topography is shown. Black lines mark the converted phase at the Moho discontinuity (Pms, dashed line is the expected continuation of the arrival according to PmsPs). Green lines show intracrustal conversions. Shaded boxes enclose the arrival time of Moho multiples (PmsPs). The vertical dashed lines mark the limit between the main geologic domains at the surface and purple dashed lines show the main fault contacts. The inset shows the locations (blue stars) of the earthquakes used in the RF analysis recorded in the temporary experiment. Abbreviations: IM, Iberian massif; EZP, Prebetic External Zones; EZS, Subbetic External Zones; IZ: Internal Zones; GB: Guadalentin Basin; CVF, Crevillente Fault; AMF, Alhama de Murcia Fault, PF Palomares Fault). (For interpretation of the references to colour in this figure legend, the reader is referred to the web version of this article.)

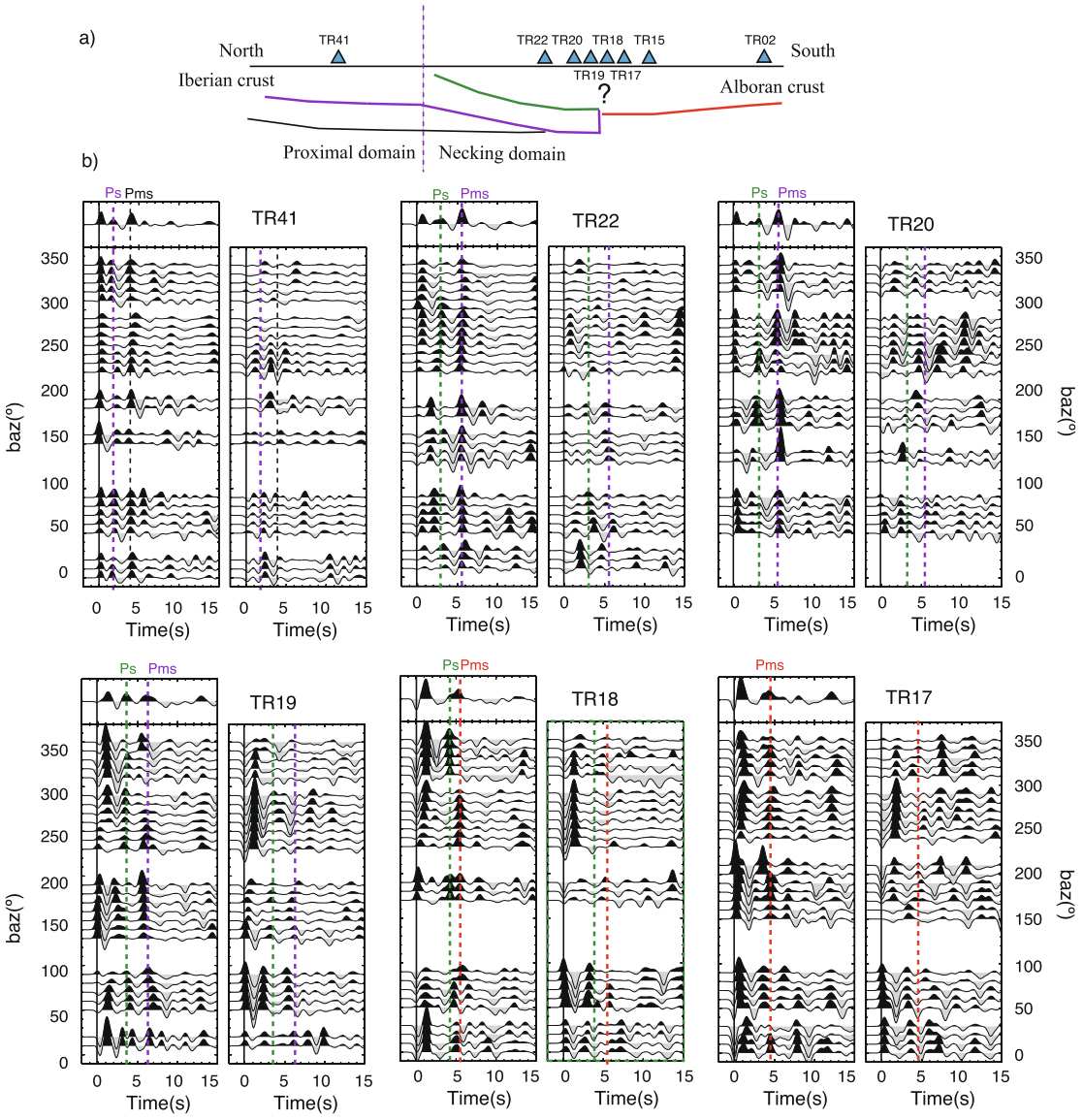

Fig. 3. a) Simplified sketch of our interpretation of the crustal structure along the profile with the location of some representative stations. b)-c) For these stations, we show the Q (left panels) and T-components (right panels) of RFs, stacked by backazimuth in bins of 10° with overlap of 5°. The summation trace of Q-components is displayed on top. All traces have been corrected by Ps moveout prior to stacking. The dashed lines mark the arrival times for the converted phase at different crustal discontinuities. Their colour refers to the discontinuity marked in a).

convert delay time to depth (see Díaz and Gallart, 2009, for a review).

In order to enhance the signal to noise ratio of the image and make better use of the high frequency information, we additionally apply a multi-signal processing to the receiver functions profile, using a post-staking processing sequence typical of reflection seismics (Yilmaz, 2001). The goal of the post-stack processing is to increase the quality of the seismic section; which entails two aspects: first, increasing the coherence of the amplitudes between adjacent traces (RFs), and on the other hand, enriching the traces with a wider bandwidth of frequencies (Teixidó, 2000). We therefore convert the original section represented in amplitude mode to traces, and apply commercial seismic processing software to the data (Globe Claritas soft code, www.globeclaritas.com). The post-processing sequence includes spatial and temporal resampling (increasing the temporal sampling from Δt = 100 ms to Δt = 12.5 ms, and duplicating the number of traces), deconvolution with a zero-phase wavelet (spike) to enhance the high frequencies, and coherence filtering by means of horizontal amplitude algorithms. Finally, a correction for spherical divergence has been applied to enhance the amplitudes in the deeper part of the section. In Fig. 4, we compare the traditional amplitude representation of the CCP stack (Fig. 4a) with the post-processed section (Fig. 4e), as well as overlay of amplitude and trace representations with different weights (Fig. 4b–d). Trace representation and post-processing enhances the coherence of the image and highlights high frequency information as intended, while preserving the position of converters. The overlay of both representations shows to be advantageous for the identification and tracking of structures, as well as to clarify their geometrical relationship with each other.

3. Results and discussion

As expected from the complex appearance of individual RFs (Fig. 3) and stacked RFs at each station (Fig. 2), the migrated receiver function section (Fig. 5) contains numerous converters, which may be related to the Moho and different intracrustal discontinu-

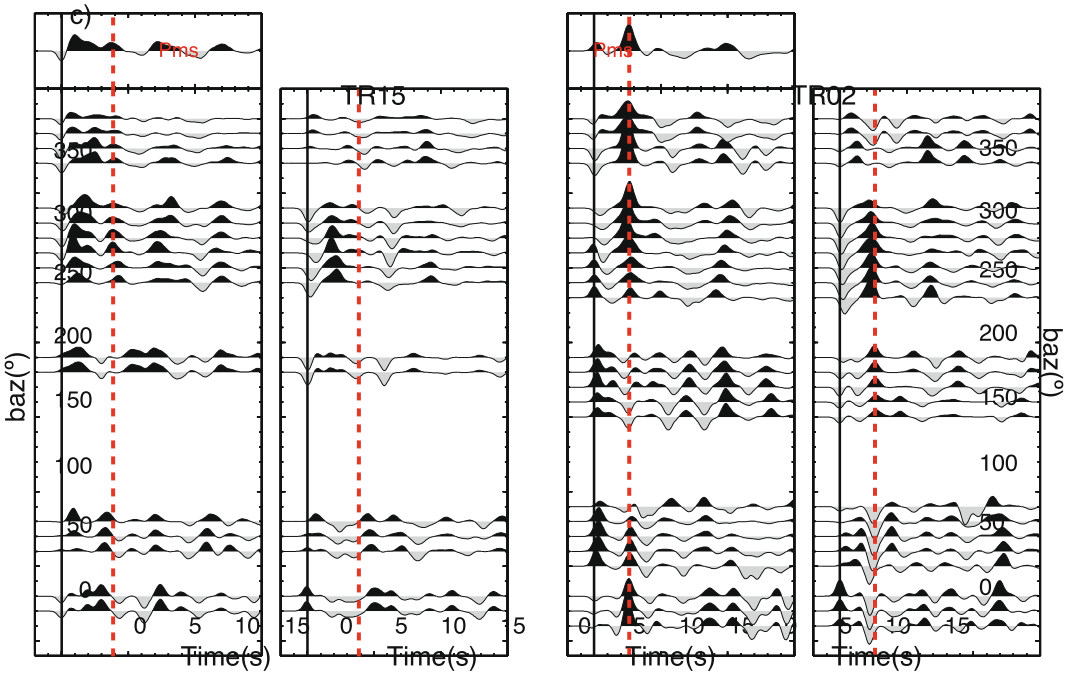

Fig. 3 (*continued*)

ities. Some of the most energetic arrivals can be characterized already from the unmigrated section of stacked RFs (Fig. 2), which present generally high signal-to-noise ratio, and show clearly several principal structures inside the orogen. The most prominent converter on the SE side of the profile can be associated with the Alboran Moho, with delay times of the converted phase, Pms, between ~2.5 s at the coast (MAZA) and ~4 s at the boundary between the External and Internal Zones. After migration, this corresponds to depths from ~20 km to ~31 km for the NW-dipping Alboran Moho in this sector (Fig. 5). At delay times between 9 s and 12 s, the first crustal multiple (PmsPs) of the Alboran Moho is visible in several stacked RFs (grey transparent area in Fig. 2). In the central part of the profile, from station TR15 to TR19 (Crevillente Fault Zone), several converters can be identified, however their geometrical relationship remains unclear from stacked RFs only (Fig. 2). In turn, from station TR20 to the NW termination of the profile, stacked RFs again are characterized by continuous arrivals (Fig. 2).

On the NW side, we can easily follow the Variscan Iberian Moho converted phase (Pms) as it becomes progressively deeper, from ~4 s delay time in the foreland domain to > 5 s under the orogen (Fig. 2). After migration, this translates to a depth range from ~30 km to ~45 km depth (Fig. 5). Variations in Bouguer gravity along the profile (Ayala et al., 2016) reproduce the trend of Moho depth variations interpreted from the receiver function transect. Bouguer gravity decreases continuously from the Iberian foreland towards a broad minimum northwest of the inferred tear fault, showing anticorrelation with the progressive increase of Moho depth (Fig. 5). At the tear fault the trends of Moho depth and Bouguer gravity are reversed, reflecting the crustal thinning towards southeast of the Alboran domain.

On the NW side, two continuous intracrustal discontinuities emerge (green lines in Fig. 2). The shallower one, according to geometry and position, may be associated with the main thrust interface of the Betic mountain range onto Iberia. RFs suggest that this contact is very shallow in the Prebetic Zone, and progressively deepening beneath the Subbetic Zone, reaching ~20 km in its deepest part. The second intracrustal discontinuities represents the prolongation of a prominent mid-crustal discontinuity broadly detected in intraplate Iberia (Simancas et al., 2003, Martínez Poyatos et al., 2012, Mancilla et al., 2015a, Ayarza et al., 2021), and associated with the intrusion of mafic sills (Brown et al., 2012). This inherited Paleozoic marker horizon allows us to distinguish between thickness variations in upper and lower Iberian continental crust. We observe convergence between the mid-crustal discontinuity and the Iberian Moho, which indicates that the lower Variscan crust is thinning progressively beneath the Betic range (Figs. 2 and 5). In turn, the total thickness of the upper crustal thickness above the marker horizon is nearly preserved in this sector, within the resolution limit of receiver functions and uncertainties of migration velocities.

We recognize this pattern of crustal thickness variations as characteristic for passive continental margins (Ranero and Pérez-Gussinyé, 2010, Huismans and Beaumont, 2011), and interpret the geometry of mid-crustal and Moho converters beneath the profile as reference to the proximal and necking domains of the Iberian paleomargin. The proximal domain, with no systematic trend in lower crustal thickness, may extend at least to station SESP, at about 10 km distance from the limit between Prebetic and Subbetic Zones at the surface (Fig. 5). Further southeast, the time difference between mid-crustal and Moho converters decreases, until both signals merge into one single pulse in the RFs between stations TR24 and TR20, suggesting the disappearance of the thinned lower crust in this sector (Fig. 2). Apparently, proximal and necking domains of the Tethys margin are still completely preserved below the Betic orogen (Figs. 2 and 5). Their position at the base of the crust indicates that the Iberian lower crust was not reworked during formation of the eastern Betics.

In the CCP stack section (Fig. 5), we can observe more detail of crustal structure. In particular, we can follow more easily the Iberian paleomargin under the orogen. In the proximal domain of the margin, we can identify sharp offsets of the Variscan mid-crustal discontinuity (near TR34, TR36 and TR41), probably indicating the positions of major normal faults that were active during crustal breakup. Interestingly, these inherited structures seem to control the length of Alpine overthrusting, as the external Betic thrust

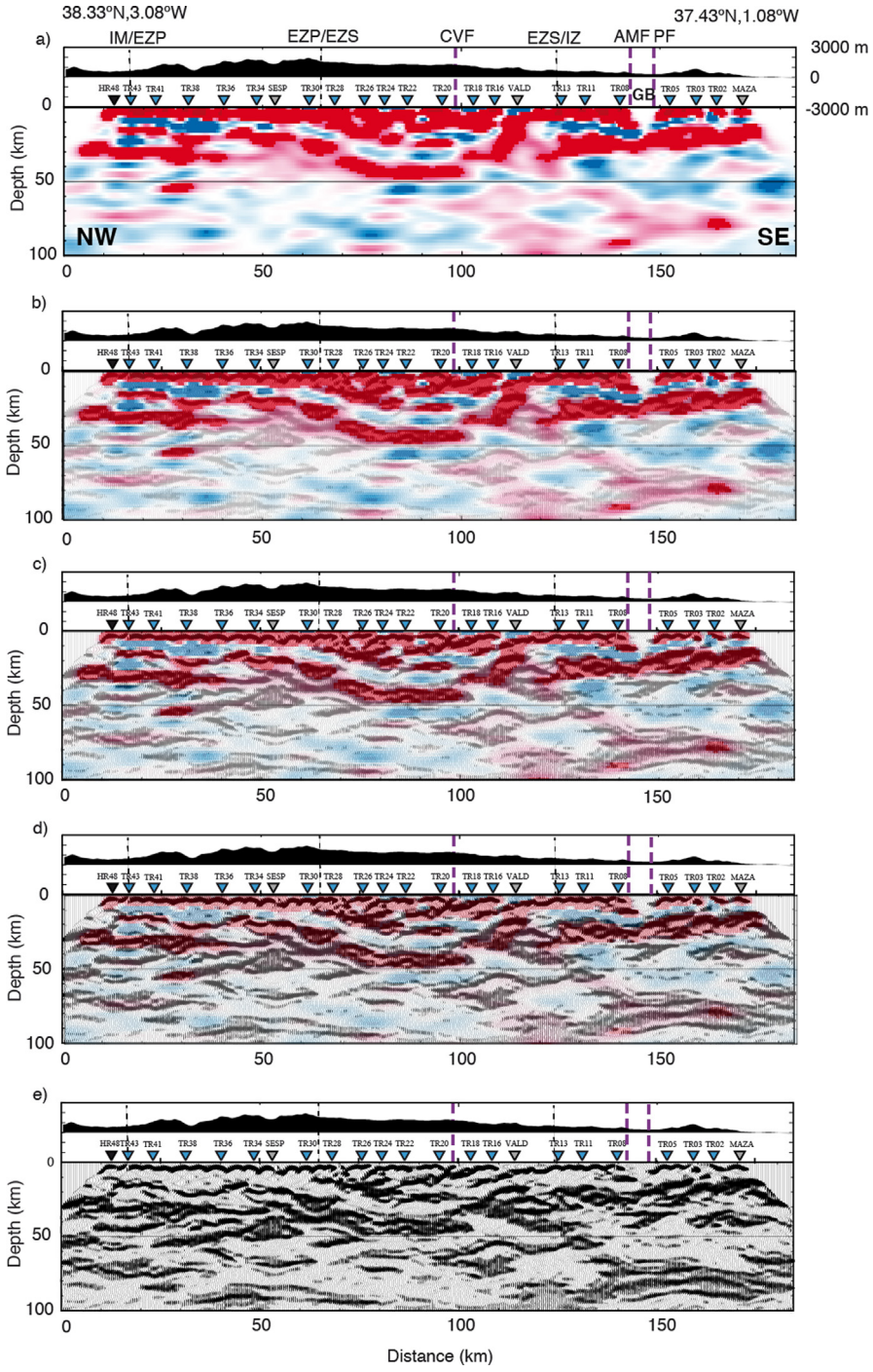

Fig. 4. Migrated RFs section (CCP stack) and post-stack trace representation along the TransCorBe profile. Overlay of amplitude and trace representation for different weights: a) weighting 1:0, b) 0.8/0.2, c) 0.6/0.4, d) 0.4/0.6 and e) 0:1. Frequency content and coherence of the trace representation were enhanced with post-processing techniques from reflection seismics (see text). Abbreviations: IM: Iberian massif; EZP: External Zones Prebetics; EZS: External Zones Subbetics; IZ: Internal Zones; GB: Guadalentin Basin (no stations were deployed inside the basin due to high noise); CVF: Crevillente Fault, AMF: Alhama de Murcia Fault, PF: Palomares Fault.

front coincides with one of the faults. Normal faulting implies that crustal thinning affected also the upper Variscan crust. The migrated section confirms a general dichotomy of compressional and extensional tectonic elements in the architecture of the Betic Range, with the inherited thrusting structure preserved on top of the Tethys paleomargin, and doming and exhumation characterizing the inner part of the orogeny (directions mark in Fig. 5 by black arrows).

The migrated image confirms convergence between mid-crustal and Moho converters and the progressive wedging of the lower crust along the ~50 km wide necking domain of the margin. Crustal thinning in this sector is very unevenly partitioned between lower and upper crust, the latter maintaining nearly constant thickness. Extension of the upper crust may have been compensated by sedimentation, or occurred predominantly in the distal domain, similar to in situ examples of Mesozoic passive margins

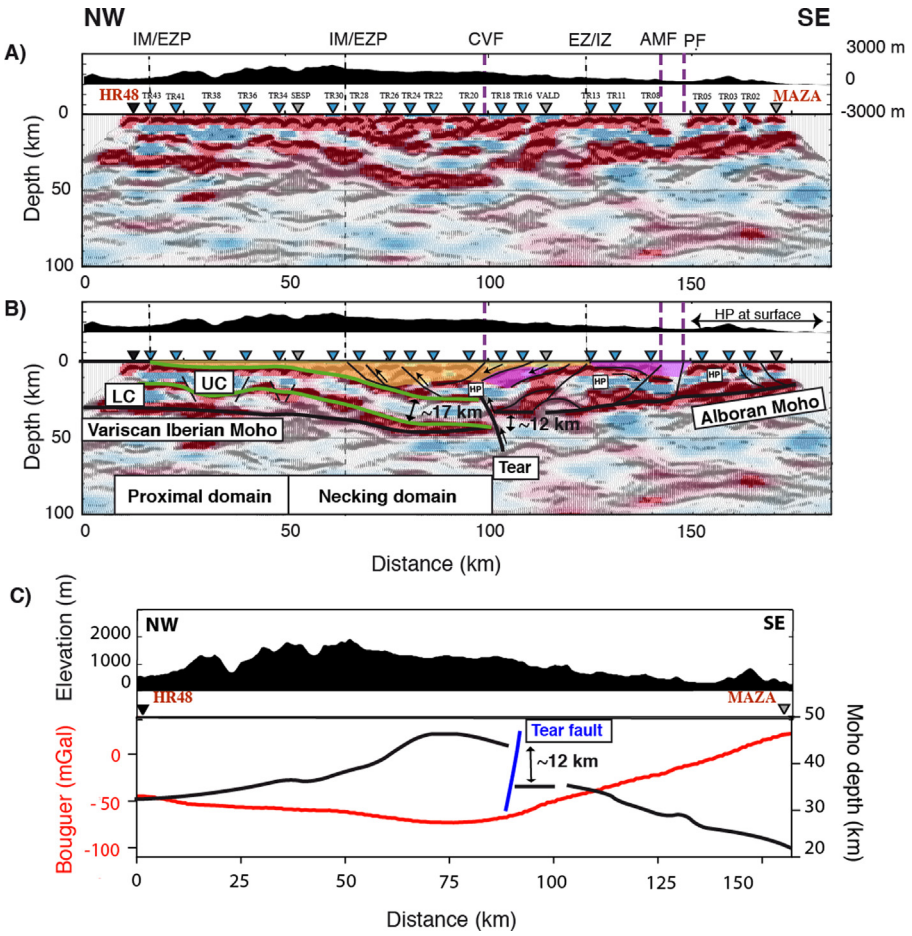

Fig. 5. A) Migrated RF section (CCP stack) along the TransCorBe profile. Overlay of amplitude and trace representation (weighting 1:1; compare Fig. 4). B) Interpreted section with crust-mantle boundary (Iberian and Alboran Moho and tear fault, thick black lines), Variscan converters (green lines; UC: upper Variscan crust; LC: lower Variscan crust), other intracrustal structures (faults and domes, thin black lines), external Betics (yellow shading), supposed or confirmed (at SE end of profile) HP units in the internal Betics, as well as probable Alboran units (magenta). Vertical black dashed lines show the contact between domains at the surface (IM: Iberian Massif Zone; EZP: Prebetic External Zone; EZS: Subbetic External Zone; IZ: Internal Zones). Purple dashed lines show the main fault contacts (CVF: Crevillente Fault; AMF: Alhama de Murcia Fault and PF: Palomares Fault). C) Bouguer gravity along the profile (red line, Ayala et al., 2016) versus Moho depth interpreted from the migrated RF section (black). (For interpretation of the references to colour in this figure legend, the reader is referred to the web version of this article.)

(e.g. Biari et al., 2017, Ros et al., 2017, Pérez-Gussinyé, 2013). The preserved Iberian paleomargin terminates abruptly at what we interpret as the distal limit of the necking zone, where the lower crust thinned out to zero thickness. Beyond this point, marked by a prominent Moho step of ~12 km vertical offset, we may associate the lowermost converter in the section with the Alboran Moho. The position of the Moho step agrees with the trail of a major, lithospheric scale tear fault that can be followed over SE-Spain, and that may have disconnected the subducting margin at this point (Fig. 1, Mancilla et al., 2015b, 2018). The observed configuration seems plausible from a mechanical point of view. Beyond the necking zone, the brittle coupling of hyperextended continental crust and mantle permits serpentinization of mantle rocks in the upper 5 km (Sutra et al., 2013), provoking mechanical weakness that may localize the initiation and propagation of slab detachment.

The central portion of the profile shows numerous medium-scale converters with variable dip and complex configuration. Compared to the unclear image of this sector in the section of stacked RFs (Fig. 2), migration is capable of unraveling the geometric relationship of the structures (Fig. 5), drawing a general picture of fault-bounded blocks as the dominant constituent of the mountain range. The crustal architecture resembles receiver function migrations from the HiRe transect further west (black triangles in Fig. 1, Mancilla et al., 2018), dominated by crustal-scale strike-slip faults and flower structures inside the Betics (in Fig. 6 both profiles are compared). This appearance is in agreement with the evolution of the Betic range and in particular the motion of the Alboran domain, where lateral transport in direction of slab rollback has been far more significant than convergence with Iberia (Spakman et al., 2018). Along the migrated section of the TransCorBe profile, the polarity pattern within several fault bounded blocks shows striking similarity with the Iberian foreland domain and the buried Iberian margin: It reproduces the same characteristic sequence of two successive sign changes (positive–negative-positive) in the upper crust. This analogy provides substantial support for recent tectonometamorphic models that associate the Nevado-Filabride unit to the continental subduction of the hyperextended Iberian paleomargin, with a provenance of this unit from the upper Iberian crust (Booth-Rea et al., 2005; Gómez-Pugnaire et al., 2012; Jabaloy-Sánchez et al., 2018).

These observations allow conjecturing about the fate of the distal domain of the Iberian paleomargin. Part of the material should have subducted, or sunk into the mantle after a major tearing event disconnected the Tethys margin at the distal limit of the necking zone. Other parts of the distal domain, in turn, have been reworked and integrated into the Betic Range. Blocks of upper continental crust from the hyper-extended margin were subducted to HP-LT conditions, exhumed along the subduction channel (e.g. Warren

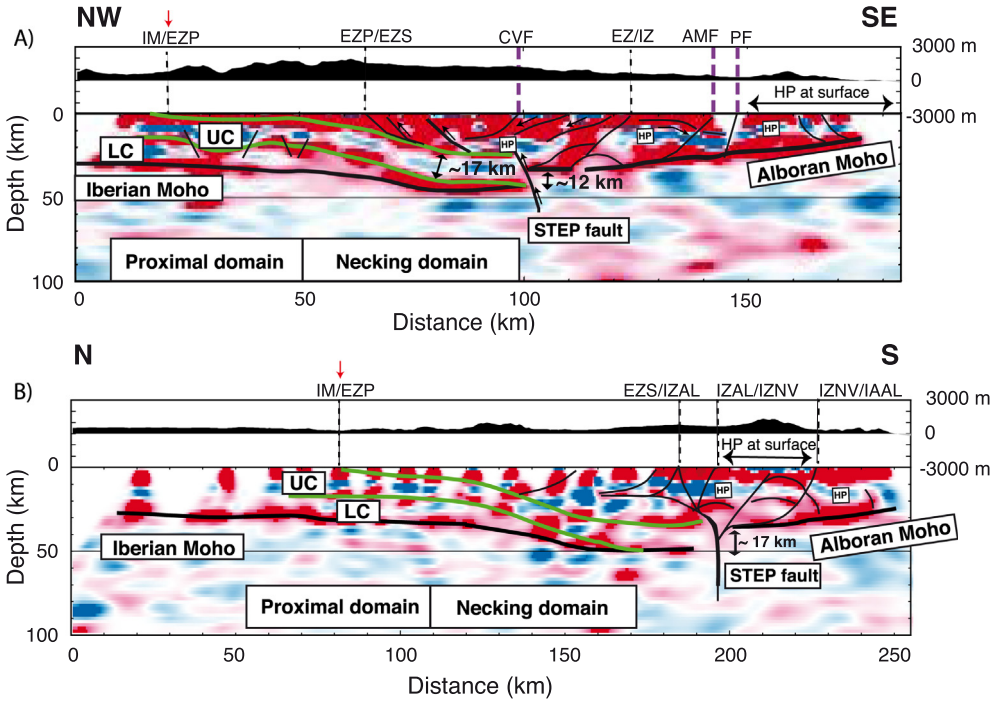

Fig. 6. Comparison of interpreted migrated RF sections (CCP stack) along the TransCorBe profile (A, blue triangles in Fig. 1) and reinterpretation of the Hire profile (B, black triangles in Fig. 1, Mancilla et al. 2018). The crust-mantle boundary (Iberian and Alborán Moho) and tear fault are marked with thick black lines, Variscan converters with green lines; faults and intracrustal converters in external Betics and Alboran domain with thin black lines. Black dashed lines show the contact between domains at the surface. Abbreviations: UC: upper Variscan crust; LC: lower Variscan crust; IM, Iberian massif; EZP, Prebetic External Zones; EZS, Subbetic External Zones; IZ: Internal Zones; IZAL: Alpujarride Internal Zone; IZNV: Nevado-Filabride Internal Zone; GB: Guadalentin Basin; CVF, Crevillente Fault; AMF, Alhama de Murcia Fault, PF Palomares Fault). (For interpretation of the references to colour in this figure legend, the reader is referred to the web version of this article.)

et al., 2008) and emplaced at the base of the orogen. A possible allocation of Iberian HP-LT units in the migrated section (Fig. 5) involves several of the main crustal blocks in the cross section. We can validate this hypothesis directly at the SE end of the profile, where the Iberian HP-LT units inferred according to the characteristic polarity pattern of Iberian crust correspond accurately to the mapped Nevado-Filabride outcrops (Fig. 1). Given the transport direction perpendicular to the profile during slab rollback, we cannot reconstruct the width of the paleomargin from the migrated section. According to the burial depth of exhumed continental HP-LT rocks, we can postulate that at least 30 km of highly thinned continental crust were present in the distal domain of the margin. Certainly, the abundance of the Iberia-type polarity pattern in the Betics suggests that the total width of the hyperextended continental margin was larger.

The identification and characterization of the Iberian paleomargin beneath the TransCorBe profile provides clues to understand intracrustal converters also in the HiRe profile, another passive seismic broad-band transect crossing the Betic Range in N-S direction and connecting with TransCorBe at its northern termination (Figs. 1 and 6). The migrated receiver function section from the HiRe profile (Mancilla et al., 2018) shows a larger vertical offset of ~17 km between the Iberian and Alboran Moho (Fig. 6), with this difference corresponding mainly to the deeper position of the Iberian Moho (~48 km), while the maximum depth of the Alboran Moho is the same in both profiles (~31 km). The presence of fault-bounded blocks on top of the STEP fault is noticeable in both profiles, including the reappearance of the characteristic polarity pattern of the Iberian upper crust in several blocks of the HiRe profile, in this case coincident with the mapped Nevado-Filabride outcrop in Sierra Nevada, and providing further support for the integration of exhumed Iberian HP-LT rocks in the Internal Betics. The coarser station spacing of ~10 km in the northern leg of the HiRe profile makes the tracking of arrivals from the Iberian paleomargin more challenging (Mancilla et al., 2018). The comparison of both profiles, however, allows its reinterpretation and to recover the position and length of the proximal and necking domains also in the HiRe profile, confirming a width of the necking domain of ~50 km (Fig. 6, note that the apparent width of the necking domain is larger, due to the oblique orientation of the profile with respect to the Tethys stretching direction). In both profiles the distal limit of the necking domain is located ~25 km from the boundary between Internal and External Zones at the surface. A remarkable difference between the profiles is the continuity of the Iberian Moho beyond the necking domain in the HiRe transect, suggesting that a narrow band of the distal domain of the Tethys margin may be conserved in this position, and that tearing of the hyperextended Iberian paleomargin occurred ~20 km from the distal limit of the necking zone.

The comparison of the TransCorBe and HiRe profiles also points to the importance of interstation distances for reducing the non-uniqueness of structural interpretations in migrated RF sections. Despite the complexity of crustal structure, the lateral continuity of underground converters is mostly easy to follow in the southern leg of HiRe (station spacing of ~2 km) and TransCorBe (station spacing of ~3.5 km), while in the northern leg of HiRe (station spacing of ~10 km), the resolution of underground converter is coarse and large ambiguity exists in the possible connections of conversion patches between stations. Our previous interpretation of HiRe (Mancilla et al., 2018) suggested a more abrupt termination of the lower crust. Along TransCorBe, we can support our structural interpretation of the paleomargin by two clear observations from the migrated section: The continuity of the upper Variscan crust, with characteristic polarity pattern and approximately constant thickness, from the Iberian foreland to the tear fault, and the convergence between the mid-crustal and Moho converters towards the tear fault. Lower crustal thinning at the margin seems to be the most likely and simplest structural model to explain both observations.

4. Conclusions

Receiver function imaging led to the discovery of the Iberian Tethys paleomargin, with intact proximal and necking domains preserved at the base of the eastern Betics, and exhumed material from the distal domain integrated inside the orogen. The general characteristics of the paleomargin resemble the magma-poor margin with serpentinized mantle preserved in situ at the Atlantic side of Variscan Iberia (Ranero and Pérez-Gussinyé, 2010, Pérez-Gussinyé, 2013, Peron-Pinvidic et al., 2013), as well as the substantially reworked fossil Tethys margin in the Alps (Mohn et al., 2012). Exhumed Iberian upper crust from the hyperextended margin is a principal constituent of the Betic range, which after rollback extension and denudation is reaching at present similar, or even greater importance than the allochthonous Alboran units themselves. The migrated section confirms a general dichotomy of compressional and extensional tectonic elements in the architecture of the Betic Range, with the inherited thrusting structure preserved on top of the Tethys paleomargin, and doming and exhumation characterizing the inner part of the orogen.

5. Author statement

J. Morales is the responding author and has prepared the text and contributed significantly to the interpretation. A. Molina-Aguilera is responsible of the P-wave receiver function analysis helped by F. Mancilla. T. Teixidó is responsible of post-stacking analysis of P-Receiver function. F. Mancilla, D. Stich, J.M. Azañon, J.A. López-Comino, X. Yuan, B. Heit and A.M. Posadas contributed significantly to the interpretation. All authors participated in discussions and contributed to the manuscript.

Declaration of Competing Interest

The authors declare that they have no known competing financial interests or personal relationships that could have appeared to influence the work reported in this paper.

Acknowledgments

We are grateful to the staff involved in the TransCorBe project. The Geophysical Instrument Pool at GFZ-Potsdam provided most of the seismic equipment. We are grateful to Christian Haberland for his support. We want to thank two anonymous reviewers for the careful reading of the manuscript and the interesting and constructive criticism they provided. This work was funded by the Spanish State Research Agency (SRA) under the grant PID2019-109608GB I00/SRA/10.13039/501100011033, FEDER/MINECO project CGL2015-67130-C2-2-R, FEDER/Junta de Andalucía project A-RNM-421-UGR18 and research group RNM104 of the Junta de Andalucía. The Granada University/CBUA funding for open access charge.

References

Augier, R., Agard, P., Monié, P., Jolivet, L., Robin, C., Booth-Rea, G., 2005. Exhumation, doming and slab retreat in the Betic Cordillera (SE Spain): in situ 40Ar/39Ar ages and P-T-d-t paths for the Nevado-Filábride complex. J. Metamorph. Geol. 23, 357–381.

Ayala, C., Bohoyo, F., Maestro, A., Reguera, M.I., Torne, M., Rubio, F., Fernàndez, M., García-Lobón, J.L., 2016. Updated Bouguer anomalies of the Iberian Peninsula: a new perspective to interpret the regional geology. J. Maps 12 (5), 1089–1092. https://doi.org/10.1080/17445647.2015.1126538.

Ayarza, P., Martínez Catalán, J.R., Martínez García, A., Alcalde, J., Andrés, J., Simancas, J.F., Palomeras, I., Martí, D., DeFelipe, I., Juhlin, C., Carbonell, R., 2021. Evolution of the Iberian Massif as deduced from its crustal thickness and geometry of a mid-crustal (Conrad) discontinuity. Solid Earth 12, 1515–1547. https://doi.org/10.5194/se-12-1515-2021.

Balanyá, J.C., García-Dueñas, V., 1987, Les directions structurales dans le Domaine d'Alborán de part et d'autre du Détroit de Gibraltar. C. R. Acad. Sci. Paris, Ser. II304, 929–932.

Behr, W.M., Platt, J.P., 2012. Kinematic and thermal evolution during two-stage exhumation of a Mediterranean subduction complex. Tectonics 31 (TC4025).

Biari, Y., Klingelhoefer, F., Sahabi, M., Funck, T., Benabdellouahed, M., Schnabel, M., Reichert, C., Gutscher, M.-A., Bronner, A., Austin, J.A., 2017. Opening of the central Atlantic Ocean: Implications for geometric rifting and asymmetric initial seafloor spreading after continental breakup. Tectonics 36, 1129–1150. https://doi.org/10.1002/2017TC004596.

Booth-Rea, G., Azañón, J.M., Martínez-Martínez, J.M., Vidal, O., García-Dueñas, V., 2005. Contrasting structural and P-T evolution of tectonic units in the southeastern Betics: key for understanding the exhumation of the Alboran Domain HP/LT crustal rocks (western Mediterranean). Tectonics 24. https://doi.org/10.1029/2004TC001640 (TC2009).

Booth-Rea, G., Jabaloy-Sánchez, A., Azdimousa, A., Asebriy, L., Vílchez, M. V., and Martínez-Martínez, J. M., 2012, Upper-crustal extension during oblique collision: The Temsamane extensional detachment (Eastern Rif, Morocco): Terra Nova, v. 24, no. 6, p. 505-512.

Booth-Rea, G., Ranero, C., Martínez-Martínez, J.M., Grevemeyer, I., 2007. Crustal types and Tertiary tectonic evolution of the Alborán sea, western Mediterranean. G-Cubed 8, Q10004.

Braga, J.C., Martin, J.M., Quesada, C., 2003. Patterns and average rates of late Neogene-Recent uplift of the Betic Cordillera, SE Spain. Geomorphology 50 (1–3), 3–26.

Brown, D., Zhang, X., Palomeras, I., Simancas, F., Carbonell, R., Juhlin, C., Salisbury, M., 2012. Petrophysical analysis of a mid-crustal reflector in the IBERSEIS profile, SW Spain. Tectonophysics 550–553, 35–46. https://doi.org/10.1016/j.tecto.2012.05.004.

Díaz, J., Gallart, J., 2009. Crustal structure beneath the Iberian Peninsula and surrounding waters: a new compilation of deep seismic sounding results. Phys. Earth Planet. Inter. 173, 181–190. https://doi.org/10.1016/j.pepi.2008.11.008.

Dilissen, N., Hidas, K., Garrido, C. J., Kahl, W-A., López Sánchez-Vizcaíno, V., and Padrón-Navarta, J.A., 2018, Textural evolution during high-pressure dehydration of serpentinite to peridotite and its relation to stress orientations and kinematics of subducting slabs: Insights from the Almirez ultramafic massif, Lithos, 320–321, 470-489, doi.org/10.1016/j.lithos.2018.09.033.

Duggen, S., Hoernle, K., Klugel, A., Geldmacher, J., Thirlwall, M., Hauff, F., Lowry, D., Oates, N., 2008. Geochemical zonation of the Miocene Alboran Basin volcanism (westernmost Mediterranean): geodynamic implications. Contrib. Miner. Petrol. 156 (5), 577–593.

Duggen, S., Hoernle, K., Van den Bogaard, P., Garbe-Schonberg, D., 2005. Post-collisional transition from subduction- to intraplate-type magmatism in the westernmost Mediterranean: Evidence for continental edge delamination of subcontinental lithosphere. J. Petrol. 46 (6), 1155–1201.

Duggen, S., Hoernle, K., van den Bogaard, P., Rupke, L., Morgan, J.P., 2003. Deep roots of the Messinian salinity crisis. Nature 422 (6932), 602–606.

Faccenna, C., Becker, T.W., Lucente, F.P., Jolivet, L., Rossetti, F., 2001a. History of subduction and back-arc extension in the Central Mediterranean. Geophys. J. Int. 145, 809–820.

Faccenna, C., Funiciello, F., Giardini, D., Lucente, P., 2001b. Episodic back-arc extension during restricted mantle convection in the Central Mediterranean. Earth Planet. Sci. Lett. 187, 105–116.

Faccenna, C., Piromallo, C., Crespo-Blanc, A., Jolivet, L., Rossetti, F., 2004. Lateral slab deformation and the origin of the western Mediterranean arcs. Tectonics 23, TC1012.

Frassetto, A., Zandt, G., Gilbert, H., Owens, T.J., Jones, C.H., 2010. Improved imaging with phase-weighted common conversion point stacks of receiver functions. Geophys. J. Int. 182 (1), 368–374. https://doi.org/10.1111/j.1365-246X.2010.04617.x.

Frizon de Lamotte, D., Raulin, C., Mouchot, N., Wrobel-Daveau, J.C., Blanpied, C., Ringenbach, J.C., 2011. The southernmost margin of the Tethys realm during the Mesozoic and Cenozoic: Initial geometry and timing of the inversion processes. Tectonics 30, TC3002. https://doi.org/10.1029/2010TC002691.

García-Castellanos, D., Villasenor, A., 2011. Messinian salinity crisis regulated by competing tectonics and erosion at the Gibraltar arc. Nature 480 (7377), 359–U108.

García-Hernández, M., López-Garrido, A., Rivas, P., Sanz de Galdeano, C., Vera, J., 1980. Mesozoic paleogeographic evolution of the External Zones of the Betics Cordillera. Geol. Mijnb. 59, 155–176.

Gómez-Pugnaire, M.T., Rubatto, D., Fernández-Soler, J.M., Jabaloy, A., López Sánchez-Vizcaíno, V., González-Lodeiro, F., Galindo-Zaldívar, and J., Padrón-Navarta, J.A., 2012, U–Pb geochronology of Nevado–Filábride gneisses: evidence for the Variscan nature of the deepest Betic complex (SE Spain). Lithos 146–147, 93–111. http://dx.doi.org/10.1016/ j.lithos.2012.03.027.

Huismans, R., Beaumont, C., 2011. Depth-dependent extension, two-stage breakup and cratonic underplating at rifted margins. Nature 473 (7345), 74–78. https://doi.org/10.1038/nature09988.

Jabaloy, A., Gómez-Pugnaire, M.T., Padrón-Navarta, J.A., López-Sánchez-Vizcaíno, V., Garrido, C.J., 2015. Subduction- and exhumation-related structures preserved in metaserpentinites and associated metasediments from the Nevado-Filábride Complex (Betic Cordillera, SE Spain). Tectonophysics 644–645, 40–57.

Jabaloy-Sánchez, A., Talavera, C., Gómez-Pugnaire, M.T., López-Sánchez-Vizcaíno, V., Vázquez-Vílchez, M., Rodríguez-Peces, M.G., Evans, N.J., 2018. U-Pb ages of detrital zircons from the Internal Betics: A key to deciphering paleogeographic provenance and tectono-stratigraphic evolution. Lithos 318–319, 244–266. https://doi.org/10.1016/j.lithos.2018.07.026.

Langston, C.A., 1979. Structure under Mount Rainier, Washigton, inferred from teleseismic body waves. J. Geophys. Res. 84, 4749–4762.
Lonergan, L., White, N., 1997, Origin of the Betic-Rif mountain belt: Tectonics, v. 16, p. 504–522, https:// doi.org/10.1029 /96TC03937.
Ligorria, J., Ammon, C., 1999. Iterative deconvolution and receiver function estimation. Bulletin of Seismological Society of America 89, 1395–1400.
López-Sánchez-Vizcaíno, V., Rubatto, D., Gómez-Pugnaire, M.T., Tommsdorff, V., Müntener, O., 2001. Middle Miocene high-pressure metamorphism and fast exhumation of the Nevado-Filábride Complex, SE Spain. Terra Nova 13, 327–332.
Mancilla, F., Stich, D., Morales, J., Martin, R., Diaz, J., Pazos, A., Cordoba, D., Pulgar, J.A., Ibarra, P., Harnafi, M., Gonzalez-Lodeiro, F., 2015a. Crustal thickness and images of the lithospheric discontinuities in the Gibraltar arc and surrounding areas. Geophys. J. Int. 203, 1804–1820. https://doi.org/10.1093/gji/ggv390.
Mancilla, F., Booth-Rea, G., Stich, D., Pérez-Peña, J.V., Morales, J., Azañón, J.M., Martín, R., Giacomia, F., 2015b. Slab rupture and delamination under the Betics and Rif constrained from receiver functions. Tectonophysics 663, 225–237. https://doi.org/10.1016/j.tecto.2015.06.028.
Mancilla, F de L., Heit, B., Morales, J., Yuan, X., Stich, D., Molina-Aguilera, A., Azañón, J.M. and Martín, R. 2018, A STEP fault in Central Betics, associated with lateral lithospheric tearing at the northern edge of the Gibraltar arc subduction system. Earth Planet. Sci. Lett. 486, 32–40. doi.org/10.1016/j.epsl.2018.01.008
Martínez-Martínez, J.M., Soto, J.I., Balanyá, J.C., 2002. Orthogonal folding of extensional detachments: Structure and origin of the Sierra Nevada elongated dome (Betics, SE Spain). Tectonics 21, no. 3.
Martínez Poyatos, D. et al., 2012. Imaging the crustal structure of the Central Iberian Zone (Variscan Belt): The ALCUDIA deep seismic reflection transect. Tectonics 31, TC3017. https://doi.org/10.1029/2011TC002995.
Mohn, G., Manatschal, G., Beltrando, M., Masini, E., Kusznir, N., 2012. Necking of continental crust in magma-poor rifted margins: Evidence from the fossil Alpine Tethys margins. Tectonics 31, TC1012. https://doi.org/10.1029/2011TC002961.
Morales, J., Martín, J.B., Martín, R., Mancilla, F., Heit, B., Yuan, X., 2015, Passive seismic profile across the Eastern Betic and Iberian Massif (TRANSCORBE)-GFZ Data Services https://doi.org/10.14470/4U7568470291.
Pérez-Gussinyé, M., 2013. A tectonic model for hyperextension at magma-poor rifted margins: an example from the West Iberia-Newfoundland conjugate margins. Geol. Soc., London, Spec. Publ. 369 (1), 403. https://doi.org/10.1144/SP369.19.
Peron-Pinvidic, G., Manatschal, G., Osmundsen, P., 2013. Structural comparison of archetypal Atlantic rifted margins: A review of observations and concepts. Mar. Pet. Geol. 43, 21–47. https://doi.org/10.1016/j.marpetgeo.2013.02.002.
Puga, E., Díaz de Federico, A., Fanning, M., Nieto, J.M., Rodríguez Martínez-Conde, J. A., Díaz Puga, M.A., Bianchini, G., Natali, C., Beccaluva, L., 2017. The Betic Ophiolites and the Mesozoic evolution of the western Tethys. Geosciences 7, 31.
Ranero, C.R., Pérez-Gussinyé, M., 2010. Sequential faulting explains the asymmetry and extension discrepancy of conjugate margins. Nature 468 (7321), 294–299. https://doi.org/10.1038/nature09520.
Rodríguez-Cañero, R., Jabaloy-Sánchez, A., Navas-Parejo, P., Martín-Algarra, A., 2018. Linking Palaeozoic palaeogeography of the Betic Cordillera to the Variscan Iberian Massif: new insight through the first conodonts of the Nevado-Filábride Complex. Int. J. Earth Sci. (Geol Rundsch) 107, 1791. https://doi.org/10.1007/s00531-017-1572-8.
Ros, E., Perez-Gussinye, M., Araujo, M., Thoaldo Romeiro, M., Andres-Martınez, M., Morgan, J.P., 2017. Lower crustal strength controls on melting and serpentinization at magma-poor margins: potential implications for the South Atlantic. Geochem. Geophys. Geosyst. 18, 4538–4557. https://doi.org/10.1002/2017GC007212.
Santamaría-López, A., Lanarib, P., Sanz de Galdeano, C., 2019. Deciphering the tectono-metamorphic evolution of the Nevado-Filábride complex (Betic Cordillera, Spain) – A petrochronological study. Tectonophysics 767, 128–158. https://doi.org/10.1016/j.tecto.2019.06.028.
Schettino, A., Turco, E., 2010. Tectonic history of the western Tethys since the Late Triassic. GSA Bull. 123, 89–105. https://doi.org/10.1130/B30064.
Schimmel, M., Paulssen, H., 1997. Noise reduction and detection of weak, coherent signals through phase-weighted stacks. Geophys. J. Int. 130 (2), 497–505.
Simancas, F., Carbonell, R., Gonzaález-Lodeiro, F., Pérez Estaún, A., Juhlin, C., Ayarza, P., Kashubin, A., Azor, A., Martínez-Poyatos, D., Almodóvar, G.R., Pascual, E., Sáez, R., Expósito, I., 2003. Crustal structure of the transpressional Variscan orogen of SW Iberia: SW Iberia deep seismic reflection profile (IBERSEIS). Tectonics 22 (6), 1062.
Spakman, W., Chertova, M.V., van der Berg, A., van Hinsbergen, D.J.J., 2018. Puzzling features of western Mediterranean tectonics explained by slab dragging. Nature Geosci. 11 (3), 1–8. https://doi.org/10.1038/s41561-018-0066-z.
Stampfli, G. M., Borel, G. D., Marchant, R. and Mosar, J. 2002, Western Alps geological constraints on western Tethyan reconstructions. In: Rosenbaum, G. and Lister, G. S. 2002. Reconstruction of the evolution of the Alpine-Himalayan Orogen. J. Virtual Explorer 7, 75–104.
Sutra, E., Manatschal, G., Mohn, G., Unternehr, P., 2013. Quantification and restoration of extensional deformation along the Western Iberia and Newfoundland rifted margins. Geochem. Geophys. Geosyst. 14, 2575–2597. https://doi.org/10.1002/ggge.20135.
Teixidó T., 2000. Caracterización del subsuelo mediante sísmica de reflexión de alta resolución. PhD Univestity of Barcelona, Spain. http://www.tdx.cat/TDX-0630103-084025.
Vignaroli, G., Faccenna, C., Jolivet, L., Piromallo, C., Rossetti, F., 2008. Orogen-parallel extension and arc bending forced by slab tearing and toroidal flow at the junction between Alps and Apennines. Tectonophysics 450, 34–50.
Vinnik, L.P., 1977. Detection of waves converted from P to SV in the mantle. Phys. Earth Planet. Int. 15, 39–45.
Warren, C.J., Beaumont, C., Jamieson, R.A., 2008. Formation and exhumation of ultra-high-pressure rocks during continental collision: Role of detachment in the subduction channel. Geochem. Geophys. Geosyst. 9, Q04019. https://doi.org/10.1029/2007GC001839.
Yilmaz, Ö., 2001. Seismic data analysis: processing, inversion, and interpretation of seismic data. Stephen M. Doherty, editor Tulsa (Okla.), Society of Exploration Geophysicists, 2001, 1-56080-094-1 (cart.)
Yuan, X., 2000. and 21 others, Subduction and collision processes in the Central Andes constrained by converted seismic phases. Nature 408, 958–961. https://doi.org/10.1038/35050073.